

Dual exposure, two-photon, conformal phase mask lithography for three dimensional silicon inverse woodpile photonic crystals

Daniel J. Shir, Erik C. Nelson, Debashis Chanda, Andrew Brzezinski, Paul V. Braun, and John A. Rogers^{a)}

Department of Materials Science and Engineering, Frederick Seitz Materials Research Laboratory, and Beckman Institute for Advanced Science and Technology, University of Illinois at Urbana-Champaign, Urbana, Illinois 61801

Pierre Wiltzius

Department of Physics, College of Letters and Science, University of California at Santa Barbara, Santa Barbara, California 93106

(Received 6 April 2010; accepted 1 June 2010; published 7 July 2010)

The authors describe the fabrication and characterization of three dimensional silicon inverse woodpile photonic crystals. A dual exposure, two-photon, conformal phasemask technique is used to create high quality polymer woodpile structures over large areas with geometries that quantitatively match expectations based on optical simulations. Depositing silicon into these templates followed by the removal of the polymer results in silicon inverse woodpile photonic crystals for which calculations indicate a wide, complete photonic bandgap over a range of structural fill fractions. Spectroscopic measurements of normal incidence reflection from both the polymer and silicon photonic crystals reveal good optical properties. © 2010 American Vacuum Society. [DOI: 10.1116/1.3456181]

I. INTRODUCTION

Three dimensional (3D) photonic crystals are of interest due to their ability to control light in ways that would be difficult with conventional optical components.¹⁻³ Photonic crystals with woodpile geometries, in particular, have drawn much attention due to the large photonic bandgaps and relatively easy fabrication compared to diamond structures.⁴ Forming such submicron, 3D structures with the required precision, however, presents a major and long-standing engineering challenge for practical application of this class of component. Many methods⁵⁻¹⁰ have been explored, most of which use a serial patterning process or self-assembly, thereby limiting the areas that can be effectively achieved or the accessible geometries, respectively. By contrast, multi-beam interference lithography⁶ (IL) is appealing due to its flexibility in structure design and capacity for patterning large areas in a parallel fashion at high speed. The main disadvantages include an inability to form structures characterized by more than a few spatial Fourier components and generally complex fabrication setups with limited utility in manufacturing. Most previous attempts in fabricating woodpile structures using IL yielded moderate low structure quality with low normal incidence reflectivity ($\sim 25\% - 35\%$).^{11,12} Fabrication methods based on phasemasks,¹³⁻²⁰ particularly those that use conformal masks in soft, contact mode exposure geometries,¹³⁻¹⁹ avoid some of these drawbacks to provide simple routes to photonic crystals¹⁷ and even aperiodic, spatially graded or quasicrystalline structures.^{15,16} In their typical implementation, however, the structure geometries remain limited; woodpile

structures, for example, cannot be fabricated easily.^{20,21} In this article, we demonstrate a conformal phasemask approach that exploits two-photon absorption in a dual exposure mode using two separate masks, using optical effects related to those proposed in Ref. 20. We demonstrate application of this method to 3D woodpile structures. The diamondlike symmetry of the resulting crystals yields a large photonic bandgap for sufficiently large refractive index contrast.⁴ To illustrate this property, we formed polymer/air structures and then converted them into silicon/air photonic crystals through a inversion process. Both polymer and silicon photonic crystals show good optical properties, thereby suggesting that this fabrication approach could provide a competitive alternative to other techniques.

II. RESULTS AND DISCUSSION

Figure 1 provides schematic illustrations of the fabrication processes along with simulations of intensity distributions for each step. For this work, we used phasemasks made of the elastomer poly(dimethylsiloxane) (PDMS) (Dow Corning, Inc.), cast and cured over patterned photoresist defined by commercially procured deep ultraviolet projection mode photolithography on a silicon wafer. The masks served as diffraction elements to provide the required near-field intensity distributions for patterned exposure of a transparent photopolymer in a two-photon process. A unique feature of the masks is that their low modulus, elastomeric mechanical properties allow them to be placed into intimate, conformal contact with a solid layer of the photopolymer without applied force or precision mechanical stages. We refer to this technique as two-photon proximity field nanopatterning (2ph-PnP).¹³ Here we use this method in a dual exposure mode to access woodpile and other geometries that are dif-

^{a)}Electronic mail: jrogers@uiuc.edu

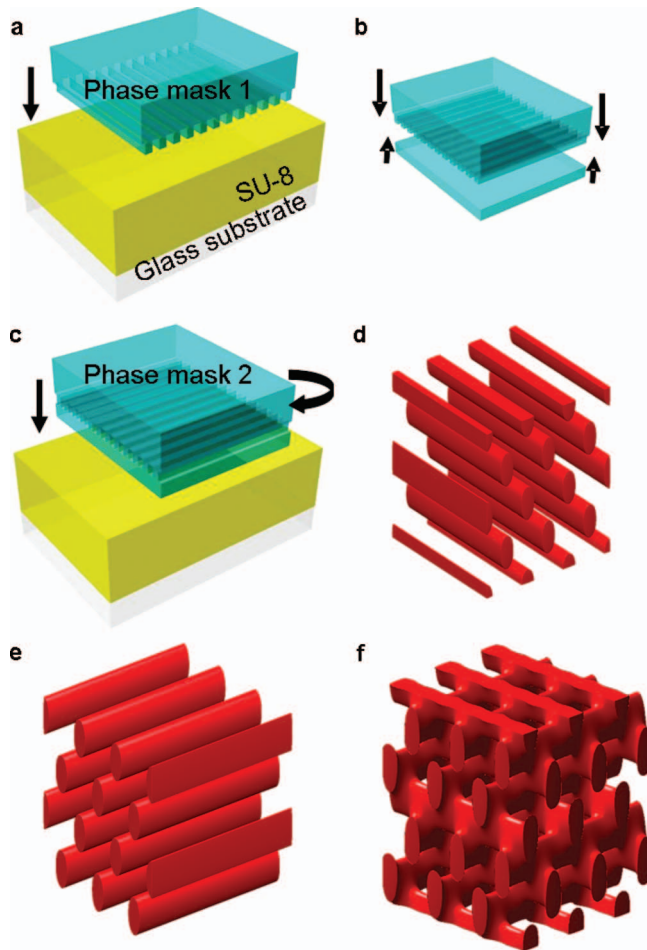


FIG. 1. (Color) Schematic illustrations of steps for two-photon, dual exposure patterning of three dimensional woodpile structures in a photopolymer, using two conformal phasemasks. (a) First and (c) second laser exposures yield arrays of rods rotated by 90° with respect to each other. (b) Illustration of the process for bonding a thin layer of PDMS to a phasemask, thereby yielding the necessary uniform optical phase shift for creating an offset by $\frac{1}{4}$ of a Talbot distance between the two sets of orthogonally rotated rods. [(d) and (e)] Simulations of structures that result from the two-photon exposure steps in (a) and (c), respectively. (f) Summed structures corresponding to both exposures.

difficult to achieve otherwise. The process is initiated by bringing a first phasemask into conformal contact with a suitable photopolymer (SU8-2010, MicroChem Inc.). Exposure with a collimated laser beam generates a rodlike intensity distribution, as shown in Fig. 1(d), with lateral and vertical spacings set by the periodicity of the mask and the Talbot self-imaging distance, respectively. To form the desired woodpile structure, a second rodlike pattern was defined in a geometry offset by $m \cdot \frac{1}{4}$ of the Talbot distance (Z_T), where m is any odd integer, with an orientation orthogonal to the first set of rods. To accomplish this, we used a second phase mask identical to the first except for the addition of a uniform capping layer of PDMS. This approach provides a simple, conformal phasemask alternative to exposures that use precision stages to control the phase shifts through mechanical positioning. This spacer layer and mask, shown in a rotated configuration, appear in Figs. 1(b) and 1(c), respectively. Figures 1(e) and

1(f) show the intensity distribution for the second exposure and the woodpile structure after combining the two intensity distributions with a binary cutoff threshold to simulate the exposure and development process. The thickness of the spacer layer is critical to the assembly of the woodpile structure because (i) it determines the spatial displacement of the two intensity patterns and (ii) it affects the intensity distribution as well as the contrast ratio of the second exposure. The second exposure should produce contrast identical to the first and place the rods exactly in the middle of the first set. Deviations in contrast can lead to uneven structure geometries. Rods that are misplaced by distances larger than 10% cause rapid decreases in the photonic bandgap of the structure.²²

The exposures were performed using an amplified Ti:sapphire laser (Spectra-Physics, Spitfire Pro) with wavelength, repetition rate, average power, and pulse width of 800 nm, 1 kHz, 2W, and ~ 140 fs, respectively. The linear polarization state was set to lie along the grating lines on the masks for both exposures, to optimize the contrast. A lens ($f = 400$ mm) with small convergence angle (< 10 mrad) was implemented at the laser output to enable peak powers sufficient to initiate two-photon effects in the photopolymer. The patterns on the phasemasks consisted of arrays of raised lines with periodicity (Λ), linewidth (lw), and relief depth (rd) of $\Lambda = 600$ nm, $lw = 300$ nm, and $rd = 220$ nm. The choice of period was based on the well known fact that a complete photonic bandgap in woodpile structures is available only in a narrow range of axial-to-transverse periodicity ratios, c/a , which in turn depend on the exposure wavelength (λ) and phasemask period (Λ).⁴ Silicon inverted woodpile structures possess a complete bandgap for c/a ratios between 0.8 and 1.5.⁴ For the present two-photon exposure laser wavelength of $\lambda = 800$ nm, $\Lambda = 600$ nm ensures a wide complete bandgap after silicon inversion of the polymer template. This value takes into account shrinkage in the polymer template that further reduces the c/a ratio close to 1.2, which provides the widest bandgap.⁴

For purpose of illustration, Fig. 2(a) compares the relative intensity of 1ph- and 2ph-PnP exposure modes, using a phasemask with a period of 600 nm and an incident wavelength of 800 nm, as a function of horizontal positions (X , perpendicular to grating direction) at a depth of 500 nm from the phasemask where the intensity contrast is the largest. The relative intensity of 1ph- and 2ph-PnP can vary depending on the distance away from the phase mask, but 2ph-PnP, in all cases, showed much larger intensity modulation compared to 1ph PnP, mostly due to the quadratic dependence of intensity associated with 2ph process. One disadvantage of using short pulses for exposure is that propagation effects limit the thicknesses of layers that can be effectively patterned. Figure 2(b) provides finite difference time domain (FDTD) simulations of propagation of a 140 fs Gaussian pulse of plane phase front through a phasemask and into an underlying polymer, where all relevant parameters match the experimental ones. Figures 2(b) and 2(c) show the 2D intensity distribution along an XZ -plane generated in the photopolymer and corre-

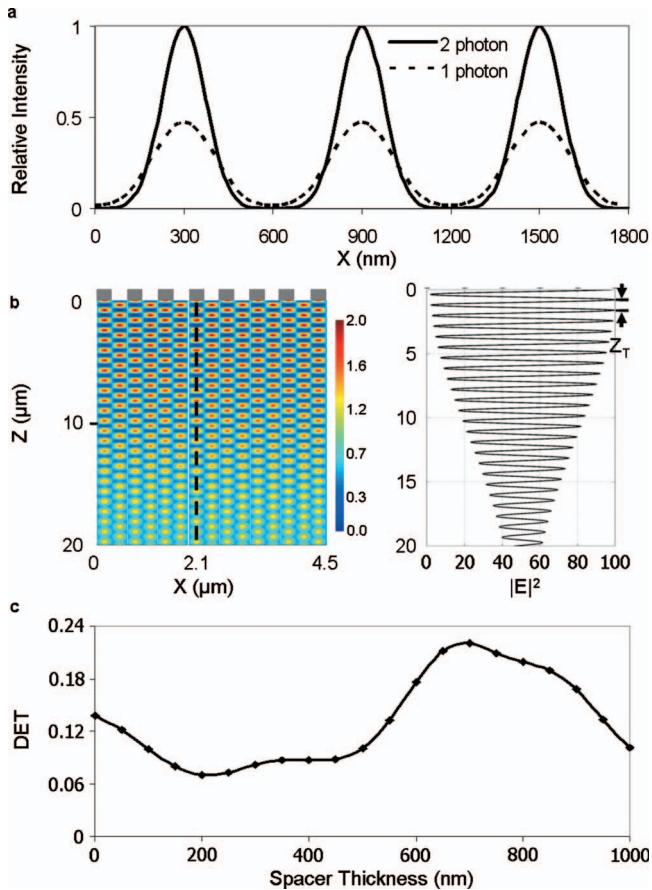


Fig. 2. (Color) (a) Simulated patterns of intensity for one- and two-photon exposures as a function of horizontal position (X , perpendicular to the grating direction) at a distance of 500 nm from the surface of the mask. (b) Pulse propagation through a one dimensional grating with Λ of 600 and rd of 220 nm, simulated using FDTD methods. The color bar indicates the relative intensity. (b) 2D Intensity distribution and (c) single line intensity profile for a fixed X -plane ($X=2.1 \mu\text{m}$). (d) Calculated diffraction efficiency (DET) as a function of spacer thickness.

sponding intensity variation for a fixed X value, respectively. The results show gradual fading of intensity contrast due to reduced interference between pulses propagating as first and zeroth order diffracted beams, mainly as a result of differences in path lengths. From Figs. 2(b) and 2(c), it is clear that for depths up to $10 \mu\text{m}$ there is a uniform intensity distribution with less than 20% variation. This result is consistent with our experimental observations of formation of uniform structures along the propagation direction up to thicknesses of $10 \mu\text{m}$.

Simulations based on rigorous coupled wave analysis revealed an elongated woodpile structure having tetragonal symmetry (TTR) with lattice parameters of $a=600 \text{ nm}$ in the plane and $c=1118 \text{ nm}$ out of the plane (i.e., vertical direction), as illustrated in Fig. 1(f). The spacer layer must separate the rodlike patterns by $m \cdot Z_T(n_s)/4 = m \cdot 206 \text{ nm}$, where m is any odd integer, and $Z_T(n_s)$ is the Talbot length in the spacer medium with refractive index n_s ($n_s=1.4$ for PDMS). As mentioned previously, the thickness of the spacer is a critically important design parameter. Figure 2(c) shows the dependence of the diffraction efficiency of the diffracted

beams on this value. η_1/η_0 corresponds to the ratio of intensity in the first order and zeroth order diffracted beams. Since the spacer thickness is comparable to the incident wavelength, it modulates the η_1/η_0 ratio through changes in intensity of the transmission and reflection beams. To produce a homogeneous (i.e., similar rod sizes for each of the two exposures) woodpile structure with high intensity contrast, we chose a spacer thickness of 618 nm, corresponding to a distance offset of $\frac{3}{4}$ of a Talbot length inside the spacer [$Z_T(n_s)$]. This layer was formed by diluting uncured PDMS with toluene (volume ratio of PDMS/toluene=1/8) and then spin casting (5000 rpm at 2500 rpm/s ramp rate for 60 s) the solution onto a silicon wafer functionalized with a fluorinated silane monolayer. Curing the layer at 55°C in a dry oven for 12 h and then bonding it to the surface of a PDMS phase mask using hydroxyl functionalization²³ completed the fabrication. Spacers formed in this way have uniform thicknesses (variations $< 10 \text{ nm}$, as measured by atomic force microscope at various locations over areas of $\sim \text{cm}^2$). Taken together, these procedures for dual exposure 2ph-PnP enable (i) high intensity contrast due to the quadratic dependence of intensity associated with two-photon process, (ii) high diffraction efficiency by use of masks with binary grating geometries and optimized depths of relief, and (iii) precise spatial, and therefore phase, control over the distance between the phase mask and the sample using soft spacers and conformal contact mode exposures.

Figure 3 presents scanning electron microscope (SEM) images of representative woodpile structures formed by procedures described in Fig. 1. Angled and high resolution top views appear in Figs. 3(a) and 3(b), respectively. The high intensity contrast of 2ph-PnP provided robust 3D structures over large areas, as shown in the angled view of Fig. 3(c). The cross-sectional view in Fig. 3(d) indicates that the rod structures have the desired offset in the vertical direction. Shrinkage in the photopolymer, well known with this material, results in a reduction in the axial period (c) in the vertical direction, in this particular exposure setup, by 25%–45%, depending on the exposure condition. Shrinkage in the lateral direction was negligible, due to adhesion to the substrate. Different exposure conditions also produce different structure fill fractions. In general, higher exposure doses produce structures with higher fill fraction and less vertical shrinkage. In this work, the fill fraction is limited to $\sim 55\%$ due to requirements of the subsequent silicon inversion process. Such fill fraction produced a vertical shrinkage of $\sim 35\%$. Variations in vertical shrinkage can create inhomogeneous structures that degrade the optical properties.²² Distortions tend to appear predominantly on the top surface due to its mechanical fragility.

Woodpile structures such as those in Fig. 3 have diamond-like symmetry with an ability to provide large photonic bandgaps (PBGs). A complete bandgap, however, is only possible when the structure consists of materials with sufficiently high refractive index contrast.⁴ To explore this possibility, we used the polymer structures described previously as templates to form Si ($n=3.6$) inverse woodpile structures

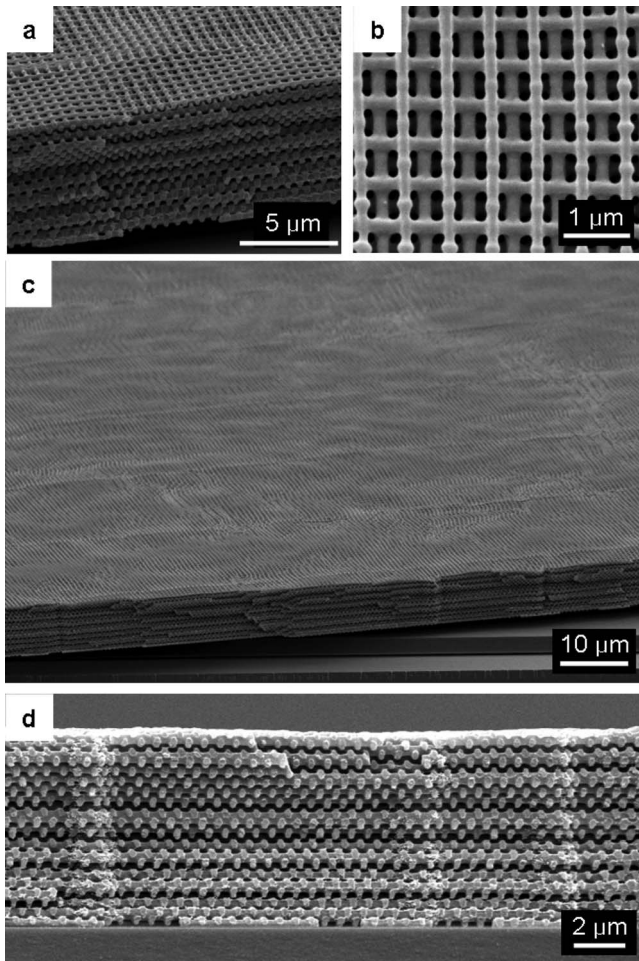


FIG. 3. SEM images of representative 3D polymer woodpile structures. [(a) and (c)] High resolution and large area angled views, respectively. (b) High resolution SEM images of the top surface. (d) SEM cross-sectional views.

using chemical vapor deposition (CVD) techniques.⁸ The inversion begins with conformal coating of Al_2O_3 onto the polymer by atomic layer deposition (ALD) to provide necessary thermal stability and control over fill fraction. Next, CVD of Si yields another conformal coating. Removing the polymer template and Al_2O_3 layer by pyrolysis and HF etching, respectively, completes the process. Growth simulations²⁴ using a template geometry shown in Fig. 4(a), with periodicities of $a=600$ nm, $c=720$ nm, and fill fraction of $\sim 55\%$, yielded quantitative information on the Si inverse woodpile structure, with results shown in Fig. 4(b). Conformal growth pinches off at $\sim 95\%$ fill fraction, leading to $\sim 5\%$ voids (isolated pores) in the Si structure. To explore the dependence of the optical properties on fill fraction, we computed the PBG (gap to midgap ratio) of Si inverse woodpile structures with different fill fractions using the University of Toronto Numerical Band Calculation Code.^{25,26} The results indicate an optimal PBG of $\sim 15\%$ at a fill fraction of $\sim 18\%$, as summarized in Fig. 4(c). The corresponding band diagram of the optimal structure appears in Fig. 4(d).

We fabricated this optimal design by first depositing 51 nm of amorphous Al_2O_3 onto the polymer template by ALD

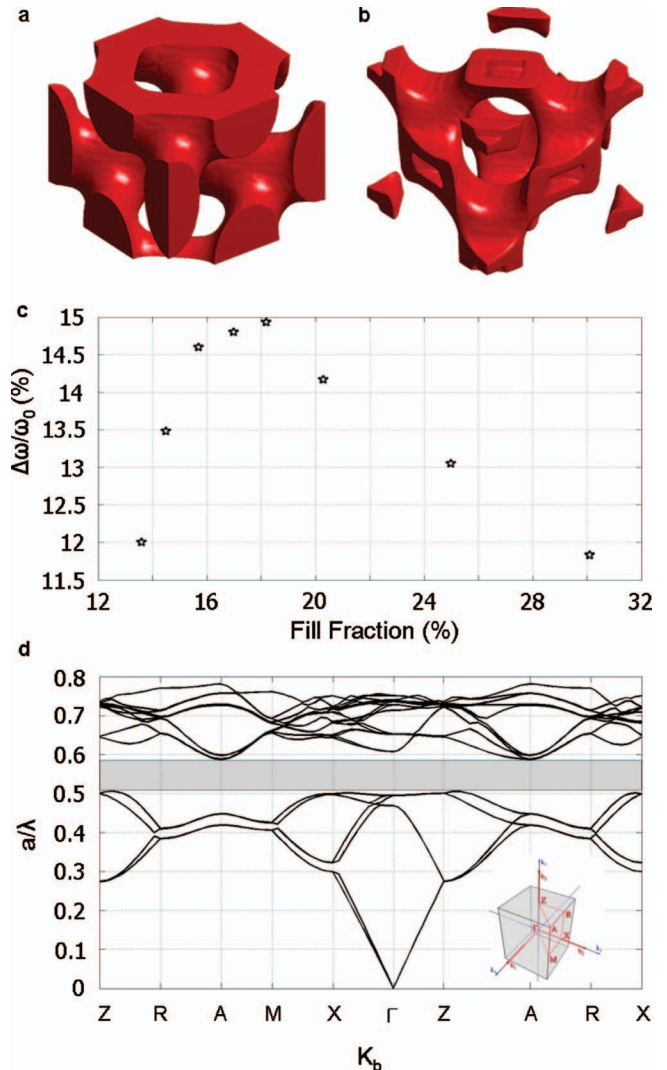


FIG. 4. (Color) Intensity simulations and photonic band calculations for an ideal woodpile structure. (a) Unit cell of a simulated polymer structure after accounting for shrinkage ($\sim 35\%$). (b) Unit cell of a simulated inverted Si structure after conformal growth simulation. (c) Gap to midgap ratio of photonic band gaps calculated at different fill fractions. (d) Photonic band diagram of the structure showed in (b) having structure periodicities of $a=600$ nm and $c=720$ nm, and Si fill fraction of 18%. The photonic band diagram showed a 15% complete photonic bandgap.

to yield a polymer/ Al_2O_3 template with a fill fraction of $\sim 77\%$. Next, amorphous silicon was conformally grown by low temperature [325°C , with 400 mbars of disilane (Si_2H_6)] static CVD. Each cycle (15 h) of silicon growth formed films with a thickness of ~ 25 nm. Three cycles (~ 84 nm) completed the infiltration step. Reactive ion etching (RIE) [3 min at 70 W, 100 mTorr, 20 SCCM (SCCM denotes cubic centimeter per minute at STP) each SF_6/O_2] removed the silicon near the top of the structure, to enable etching of the Al_2O_3 (5% HF in 50/50 ethanol/water mixture; 3 min) and subsequent removal of polymer (410°C for 4 h). Figure 5 provides the SEM images of a representative structure. Figures 5(a) and 5(b) show angled and top views. Large area angled views and cross-sectional views appear in Figs. 5(c) and 5(d), respectively. The micrographs in Fig. 5 dem-

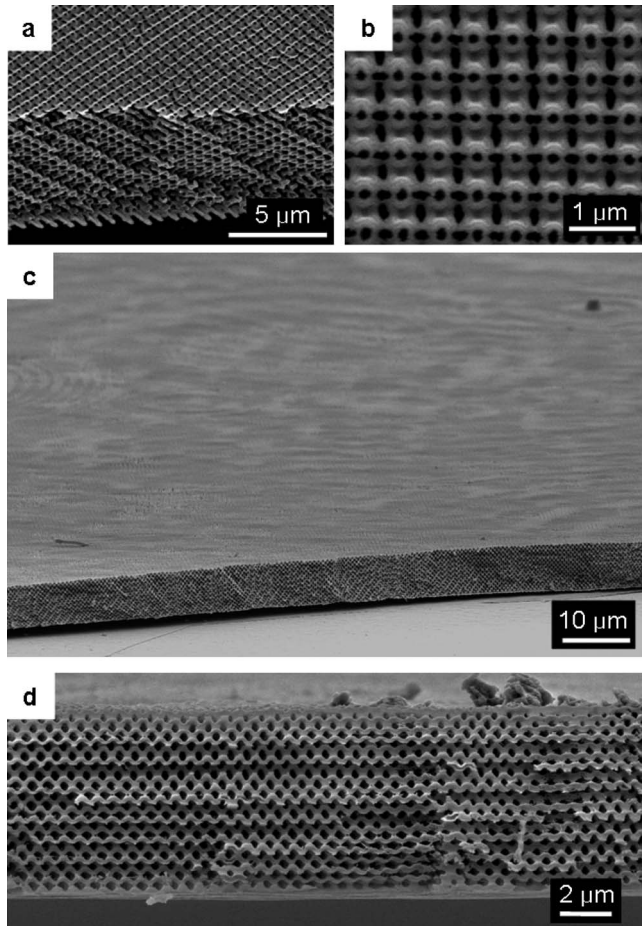


Fig. 5. SEM images of representative 3D silicon woodpile structures formed by a single inversion process. [(a) and (c)] High resolution and large area angled views, respectively. (b) High resolution images of the top surface. (d) Low resolution cross-sectional view.

onstrate that the structure is converted to silicon with high fidelity. However, structure distortions in the polymer structure can be transferred and magnified in the inverted silicon structure during the RIE and burn out processes, leading to nonuniform top surfaces.

To characterize the structural and optical properties, we performed normal incidence reflection measurements using an optical microscope (Carl Zeiss, Inc., Axio Observer D1) coupled to a spectrometer (Control Development, Inc.) and an optical microscope (Bruker Optics Inc., Hyperion 1000) coupled to a Fourier transform infrared spectrometer (Bruker Optics Inc., Vertex 70), respectively. A silver mirror with $R > 99\%$ throughout the relevant spectral range served as a reference for the reflection measurements. All spectra were collected with a 30 μm spot size obtained with a $10\times$ objective lens and a 0.3 mm spatial aperture. Figures 6(a) and 6(b) show the experimental and calculated normal incidence (Γ -Z) reflection spectra for the polymer template and silicon-air photonic crystal, respectively. Simulations were performed using the FDTD method for both the polymer template and silicon structures, as shown in Figs. 6(a) and 6(b), respectively. Periodic boundary conditions with 1 unit cell [Fig. 4(b)] along the x - y directions and perfectly matched

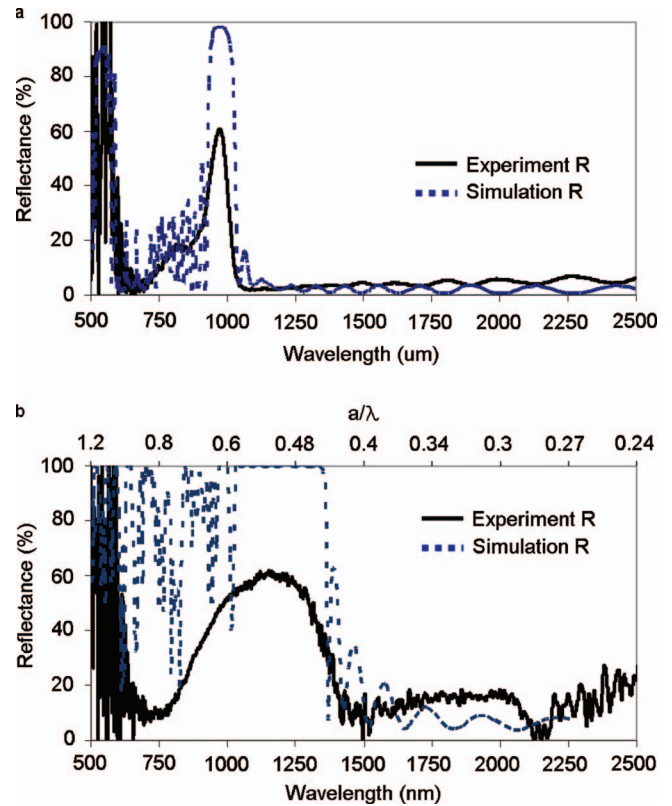


Fig. 6. (Color) Measured and simulated normal incidence (Γ -Z) reflection spectra of the polymer woodpile (a) and corresponding Si inverse woodpile (b) structure. The measured and simulated reflection peak locations ($a/\lambda = 0.55$) of the silicon inverted structure closely match the Γ -Z direction band diagram in Fig. 4(d).

layer boundary condition with 8 unit cells along the z -direction were used. The measured and simulated reflection peak location ($a/\lambda = 0.55$) of the silicon inverted structure also closely matches the Γ -Z direction band diagram in Fig. 4(d). The measured peak magnitudes of the polymer structure, i.e., $\sim 60\%$, are much better than previously reported diamondlike structures with similar number of layers obtained by interference lithography ($\sim 25\% - 35\%$),^{11,12} likely due to the comparatively high fidelity afforded by 2ph-PnP. The silicon photonic crystal shows a broad reflection peak at slightly longer wavelengths with comparable reflectance ($\sim 62\%$) to the polymer. The increase in bandwidth and the location of the reflection peak compared to the polymer template are consistent with the index of refraction of the silicon. As with the polymer template, the peak magnitude of the Si inverse woodpile structure is significantly higher than the best previous reports ($\sim 35\%$) of diamondlike silicon photonic crystals formed by interference lithography.¹² In both cases, however, the experimentally measured reflection magnitudes are somewhat smaller than those expected based on the FDTD simulation. Likewise, Fabry-Pérot fringes appear in the simulation spectra but are not prominent in the experimental data. These two aspects might result from the combination of effects such as structural imperfections, inhomogeneities due to distortions in the laser beam profile, scattering

from the rough surfaces of the samples,²⁷ and nonuniform shrinkage during the polymer development process.

III. CONCLUSION

We report a simple method for fabricating 3D woodpile photonic crystals with levels of structural uniformity and optical properties that exceed those of other approaches with parallel, high speed modes of operation. Observations suggest that the main limitations arise from materials aspects associated with exposure and development of the photopolymer, rather than from the optics or other characteristics of the dual exposure 2ph-PnP method. As such, future work on advanced, photopolymers appears to be a promising direction for research.

ACKNOWLEDGMENTS

The authors also acknowledge T. Banks and K. Colravy for help with processing using facilities at the Materials Research Laboratory. This work is supported by the DOE through Grant No. DE-FG02-07ER46471 and supported as part of the Light-Material Interactions in Energy Conversion' Energy Frontier Research Center under Grant No. DE-SC0001293. The facilities included the Materials Research Laboratory, University of Illinois, which is partially supported by the U.S. Department of Energy under Grant Nos. DE-FG02-07ER46453 and DE-FG02-07ER46471.

¹E. Yablonovitch, *Phys. Rev. Lett.* **58**, 2059 (1987).

²R. D. Meade, D. A. Devenyi, J. D. Joannopoulos, O. L. Alerhand, D. A. Smith, and K. Kash, *J. Appl. Phys.* **75**, 4753 (1994).

³J. D. Joannopoulos, P. R. Villeneuve, and S. Fan, *Nature (London)* **386**, 143 (1997).

⁴K. M. Ho, C. T. Chan, C. M. Soukoulis, R. Biswas, and M. Sigalas, *Solid State Commun.* **89**, 413 (1994).

⁵B. H. Cumpston *et al.*, *Nature (London)* **398**, 51 (1999).

⁶A. Blanco *et al.*, *Nature (London)* **405**, 437 (2000).

⁷M. Campbell, D. N. Sharp, M. T. Harrison, R. G. Denning, and A. J. Turberfield, *Nature (London)* **404**, 53 (2000).

⁸V. Ramanam, E. Nelson, A. Brzezinski, P. V. Braun, and P. Wiltzius, *Appl. Phys. Lett.* **92**, 173304 (2008).

⁹Y. C. Chen, J. B. Geddes III, J. T. Lee, P. V. Braun, and P. Wiltzius, *Appl. Phys. Lett.* **91**, 241103 (2007).

¹⁰G. M. Gratson, M. Xu, and J. A. Lewis, *Nature (London)* **428**, 386 (2004).

¹¹J. H. Moon, S. Yang, W. Dong, J. W. Perry, A. Adibi, and S.-M. Yang, *Opt. Express* **14**, 6297 (2006).

¹²Y. C. Zhong, S. A. Zhu, H. M. Su, H. Z. Wang, J. M. Chen, Z. H. Zeng, and Y. L. Chen, *Appl. Phys. Lett.* **87**, 061103 (2005).

¹³S. Jeon, J.-U. Park, R. Cirelli, S. Yang, C. E. Heitzman, P. V. Braun, P. J. A. Kenis, and J. A. Rogers, *Proc. Natl. Acad. Sci. U.S.A.* **101**, 12428 (2004).

¹⁴D. Shir *et al.*, *J. Phys. Chem. B* **111**, 12945 (2007).

¹⁵M. Maldovan, C. K. Ullal, J.-H. Jang, and E. L. Thomas, *Adv. Mater.* **19**, 3809 (2007).

¹⁶D. Shir, H. Liao, S. Jeon, D. Xiao, H. T. Johnson, G. R. Bogart, K. H. A. Bogart, and J. A. Rogers, *Nano Lett.* **8**, 2236 (2008).

¹⁷D. Shir *et al.*, *Appl. Phys. Lett.* **94**, 011101 (2009).

¹⁸S. Jeon, V. Malyarchuk, J. A. Rogers, and G. P. Wiederrecht, *Opt. Express* **14**, 2300 (2006).

¹⁹S. Jeon *et al.*, *Opt. Express* **15**, 6358 (2007).

²⁰D. Chanda, L. Abolghasemi, and P. R. Herman, *Opt. Express* **14**, 8568 (2006).

²¹D. Chanda, L. E. Abolghasemi, M. Haque, M. L. Ng, and P. R. Herman, *Opt. Express* **16**, 15402 (2008).

²²L. A. Woldering, A. P. Mosk, R. W. Tjerkstra, and W. L. Vos, *J. Appl. Phys.* **105**, 093108 (2009).

²³K. Efimenko, W. E. Wallace, and J. Genzer, *J. Colloid Interface Sci.* **254**, 306 (2002).

²⁴A. Brzezinski, Y.-C. Chen, P. Wiltzius, and P. V. Braun, *J. Mater. Chem.* **19**, 9126 (2009).

²⁵D. Chanda, M. Haque, and P. R. Herman, University of Toronto Numerical Band Calculation Code, <http://photonics.light.utoronto.ca/laserphotonics/UTNumericalBandCalculation.html>.

²⁶D. Chanda, L. Abolghasemi, and P. R. Herman, *Proc. SPIE* **6128**, 311 (2006).

²⁷M. Miyake, Y.-C. Chen, P. V. Braun, and P. Wiltzius, *Adv. Mater.* **21**, 3012 (2009).